Supplemental Material for "Spin–orbital-angular-momentum coupled Bose-Einstein condensates"

H. -R. Chen, K. -Y. Lin, P. -K. Chen, N. -C. Chiu, J. -B. Wang, C. -A. Chen, P. -P. Huang, and Y. -J. Lin*
Institute of Atomic and Molecular Sciences, Academia Sinica, Taipei, Taiwan 10617

S. -K. Yip
Institute of Physics, Academia Sinica, Taipei, Taiwan 11529 and
Institute of Atomic and Molecular Sciences, Academia Sinica, Taipei, Taiwan 10617

Yuki Kawaguchi
Department of Applied Physics, Nagoya University, Nagoya, 464-8603, Japan
(Dated: August 17, 2018)

FORMALISM OF DRESSED STATES

Hamiltonian with SOAMC

With the bias field along $\mathbf{e}_x$ and taking the conventional quantization axis along $\mathbf{e}_z$, we perform a global spin rotation, $\hat{F}_x \to \hat{F}_z, \hat{F}_y \to \hat{F}_x, \hat{F}_z \to \hat{F}_y$. We then make the rotating wave approximation, and the Hamiltonian in the bare spin basis $|+1\rangle, |0\rangle, |-1\rangle$ in the frame rotating at $\Delta\omega_L$ is

$$\begin{aligned}\hat{H}_{\rm lab} &= \left[\frac{-\hbar^2}{2m}\frac{\partial}{r\partial r}(r\frac{\partial}{\partial r}) - \frac{\hbar^2}{2m}\frac{\partial^2}{\partial z^2} + \frac{L_z^2}{2mr^2}\right]\otimes\hat{1} + \vec{\Omega}_{\rm eff}\cdot\vec{F} \\ &= \left[\frac{-\hbar^2}{2m}\frac{\partial}{r\partial r}(r\frac{\partial}{\partial r}) - \frac{\hbar^2}{2m}\frac{\partial^2}{\partial z^2} + \frac{L_z^2}{2mr^2}\right]\otimes\hat{1} + \hbar\delta\hat{F}_z \\ &\quad +\hbar\Omega(r)\cos\phi\hat{F}_x - \hbar\Omega(r)\sin\phi\hat{F}_y \end{aligned} \tag{1}$$

in the (r,ϕ,z) coordinate. Here, $\vec{\Omega}_{\rm eff} = \Omega(r)\cos\phi\mathbf{e}_x - \Omega(r)\sin\phi\mathbf{e}_y + \delta\mathbf{e}_z$ given the OAM transfer $\Delta\ell = \hbar$. We perform a local spin rotation about $\mathbf{e}_z$ by the azimuthal angle $-\phi$ to remove the $\phi-$dependence of $\vec{\Omega}_{\rm eff}$, making $\vec{\Omega}_{\rm eff}\cdot\vec{F}$ transformed to $\hbar\delta\hat{F}_z + \hbar\Omega\hat{F}_x$, and thus

$$\begin{aligned}\hat{H}_0 &= \left[\frac{-\hbar^2}{2m}\frac{\partial}{r\partial r}(r\frac{\partial}{\partial r}) - \frac{\hbar^2}{2m}\frac{\partial^2}{\partial z^2} + \frac{L_z^2}{2mr^2}\right]\otimes\hat{1} \\ &\quad +\hbar\delta\hat{F}_z + \hbar\Omega\hat{F}_x + \hat{H}_{\rm SOAMC} + \frac{\hbar^2}{2mr^2}\hat{F}_z^2, \end{aligned} \tag{2}$$

where $\hat{H}_{\rm SOAMC} = (\hbar/mr^2)L_z\hat{F}_z$. This can be expressed as

$$\hat{H}_0 = \hat{h}_0\otimes\hat{1} + \hbar\delta\hat{F}_z + \hbar\Omega\hat{F}_x + \begin{pmatrix} (L_z+\hbar)^2/(2mr^2) & 0 & 0 \\ 0 & L_z^2/(2mr^2) & 0 \\ 0 & 0 & (L_z-\hbar)^2/(2mr^2)\end{pmatrix}, \tag{3}$$

where $\hat{h}_0 = -(\hbar^2/2m)\left[r^{-1}\partial_r(r\partial_r) + \partial_z^2\right] + V(r)$, and the 3×3 matrix indicates the spin-m_F-dependent azimuthal kinetic energy $(L_z + m_F\hbar)^2/(2mr^2)$ for $m_F = \pm 1, 0$. This shows the energy dispersion for bares spin state $|m_F\rangle$ in Fig. 1c is $(L_z + m_F\hbar)^2/(2mr^2) + m_F\hbar\delta$.

Finally with a global spin rotation, $\hat{F}_z \to \hat{F}_x, \hat{F}_x \to \hat{F}_y, \hat{F}_y \to \hat{F}_z$, it gives

$$\begin{aligned}\hat{H} &= \left[\frac{-\hbar^2}{2m}\frac{\partial}{r\partial r}(r\frac{\partial}{\partial r}) - \frac{\hbar^2}{2m}\frac{\partial^2}{\partial z^2} + \frac{L_z^2}{2mr^2}\right]\otimes\hat{1} \\ &\quad +\hbar\delta\hat{F}_x + \hbar\Omega\hat{F}_y + \frac{\hbar}{mr^2}L_z\hat{F}_x + \frac{\hbar^2}{2mr^2}\hat{F}_x^2, \end{aligned} \tag{4}$$

back to the quantization axis along $\mathbf{e}_x$.

Gauge potentials

For atoms in bare spin state $|m_F = n\rangle$ and are adiabatically loaded to the dressed state $|\xi_n(\vec{r},t)\rangle$, this can be described with an Euler rotation [1] with the Euler angles (α, β, γ),

$$|\xi_n(\vec{r},t)\rangle = \mathcal{U}(\alpha,\beta,\gamma)|m_F = n\rangle, \tag{5}$$

where $n = \pm 1(0)$ is for the ferromagnetic $|\langle\vec{F}\rangle| = 1$ (polar $\langle\vec{F}\rangle = 0$) state, α and β are given by the azimuthal and polar angle of $\vec{\Omega}_{\text{eff}}(\vec{r},t)$, respectively. For the $n = \pm 1$ ferromagnetic state, γ is equivalent to the gauge choice while for the $n = 0$ polar state γ does not appear. This leads to

$$|\xi_{\pm 1}(r,t)\rangle = e^{\mp i\gamma}\begin{pmatrix} e^{-i\alpha}\frac{1\pm\cos\beta}{2} \\ \frac{\pm 1}{\sqrt{2}}\sin\beta \\ e^{i\alpha}\frac{1\mp\cos\beta}{2}\end{pmatrix}, |\xi_0(r,t)\rangle = \begin{pmatrix} -e^{-i\alpha}\frac{\sin\beta}{\sqrt{2}} \\ \cos\beta \\ e^{i\alpha}\frac{\sin\beta}{\sqrt{2}}\end{pmatrix}. \tag{6}$$

Two conventional choices of γ for the ferromagnetic state are $\gamma = 0$ and $\gamma = \mp\alpha$, where both γ and α are time-independent (see next paragraph). With these choices, the dynamical phase appears in the phase of the external part of wave function $\psi_n(r,t)$, not in $|\xi_n(r,t)\rangle$.

In our $\vec{\Omega}_{\text{eff}}(\vec{r},t)$ from the Gaussian and LG Raman beams, $\alpha = -(\Delta\ell/\hbar)\phi$ is an integer multiple of ϕ and time independent, consequently in Eq. S(6) the phase winding number (the integer given by the phase gradient along $\mathbf{e}_\phi$) of each $|m_F\rangle$ component is stationary. Besides, since $\left[H^{(n)}_{\text{eff}}, L_z\right] = 0$, the phase gradient of $\psi_n(\vec{r},t)$ along $\mathbf{e}_\phi$ remains zero and this gradient is developed with time (initially zero) only along $\mathbf{e}_r$ [2].

For our experiment where $|\Psi\rangle$ was initially polarized in $|m_F = 0\rangle$ with zero angular momentum, γ doesn't appear in $|\xi_0\rangle$ and thus the gauge potential for $|\xi_0\rangle$ is $A_0 = 0$ without additional phase term of gauge transformation. This corresponds to the conventional gauge choice of $\gamma = 0$ for $n = \pm 1$, leading to $A_{\pm 1} = \mp(\hbar/r)\cos\beta(r)$ for $|\xi_{\pm 1}\rangle$ (see the later Eq. S(7)).

3D TDGPE simulations for spin textures

We numerically simulate the dynamics by solving the three-component 3D time-dependent-Gross-Pitaevskii equation (TDGPE). We use the Crank-Nicolson method and calculate in the system size of $(256)^3$ grid points with grid size 0.22 μm. During TOF, we solve the full 3D TDGPE for up to ≤ 6 ms at which the interatomic interaction energy becomes less than 5 percent of the total energy. The further evolution is calculated by neglecting the interaction term. The results for the polar dressed state with a short hold time $t_h = 1$ ms are shown in Fig. S1, and our corresponding data is in Fig. 2.

Dressed eigenstates and validity of the adiabatic condition

The Hamiltonian $\hat{H}_0$ is dominated by the atom-light coupling $\hbar\delta\hat{F}_z + \hbar\Omega\hat{F}_x$ at large r with a sufficiently large gap $\Omega_{\text{eff}}(r) = \sqrt{\Omega(r)^2 + \delta^2}$. Thus the $\hat{H}_{\text{SOAMC}}$ and $(\hbar^2/2mr^2)\hat{F}_z^2$ originating from the gradient energy $\hat{K} \equiv -(\hbar^2/2m)\nabla^2 \otimes \hat{1}$ after the local spin rotation can be treated as perturbations.

We consider the gradient energy being projected onto the basis of local dressed states $|\xi_n\rangle$, where the off-diagonal term $H_{n'n}$ indicates coupling between dressed state n and n'. We will prove the validity of local dressed states $|\xi_n(\vec{r},t)\rangle$ as the approximated eigenstates, and of the adiabatic condition, i.e., coupling between dressed states are negligible.

Taking the Hamiltonian in Eq. S(1) and transform it to that in the basis of local dressed state $|\xi_n(\vec{r},t)\rangle$, the transformed Hamiltonian has gauge potential $\mathbf{A} = i\hbar\mathcal{U}^\dagger\nabla\mathcal{U}$ [3] with $\mathbf{A}_{n'n} = i\hbar\langle\xi_{n'}|\nabla\xi_n\rangle$,

$$\begin{aligned}\mathbf{A} &= -\frac{\Delta\ell}{r}\cos\beta(r)\hat{F}_z\mathbf{e}_\phi + \frac{\Delta\ell}{r}\sin\beta(r)\hat{F}_x\mathbf{e}_\phi + \hbar\partial_r\beta(r)\hat{F}_y\mathbf{e}_r, \\ \vec{A}_n &= \mathbf{A}_{nn} = -\frac{\Delta\ell}{r}\cos\beta(r)n\mathbf{e}_\phi,\end{aligned} \tag{7}$$

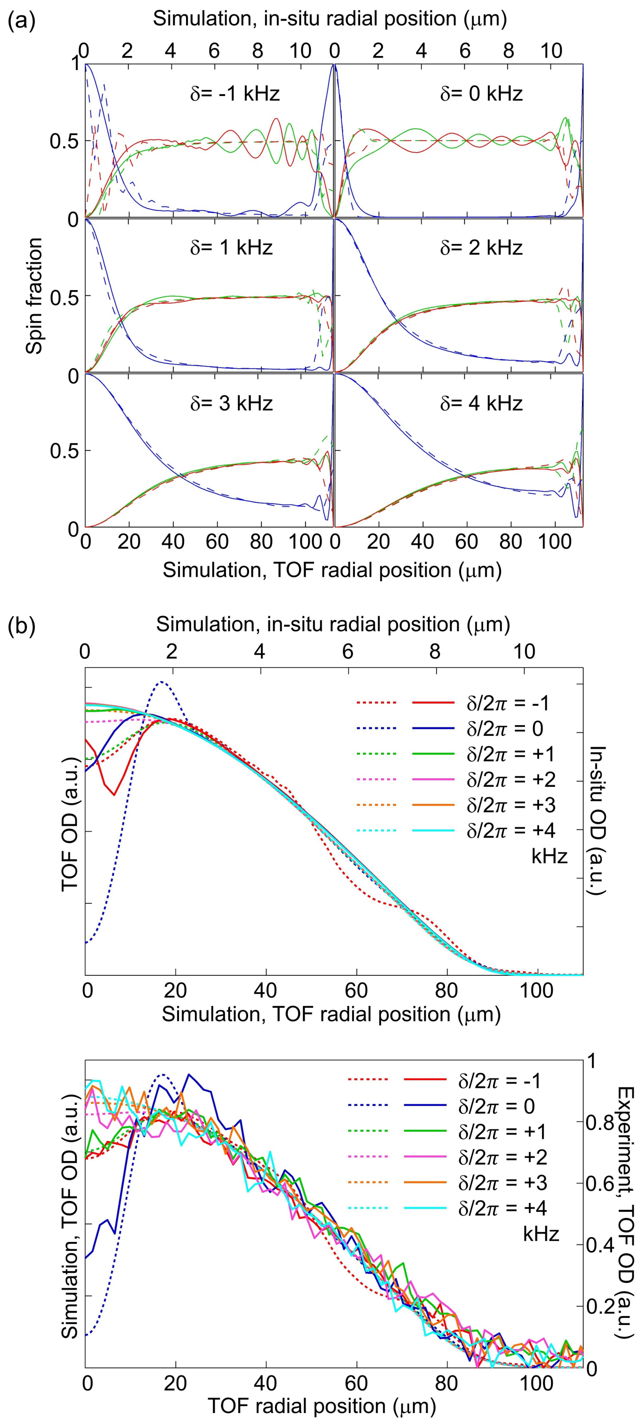

FIG. 1: 3D TDGPE simulation results for radial cross sections of polar dressed state at various detuning δ with a short hold time $t_h = 1$ ms. (a) Spin texture $D_{m_F}/(D_1 + D_0 + D_{-1})$ for in-situ (dashed curves) and for after 24 ms TOF (solid curves). Blue, red and green curves denote $|0\rangle, |1\rangle, |-1\rangle$, respectively. Except for $\delta \leq 0$, the profiles at in-situ and after TOF agree well, i.e., it is a dilation after TOF for each $|m_F\rangle$. (b) Top panel: total optical density $(D_1 + D_0 + D_{-1})$ for simulated in-situ (solid curves) and TOF profiles (dashed curves). Bottom panel: total optical density for experimental (solid curves) and simulated TOF profiles (dashed curves).

$$H_{n'n} = \frac{-\hbar}{2m}(k \cdot \mathbf{A}_{n'n} + \mathbf{A}_{n'n} \cdot k) + \frac{\mathbf{A}_{n'n} \cdot \mathbf{A}_{nn} + \mathbf{A}_{n'n'} \cdot \mathbf{A}_{n'n}}{2m}, \tag{8}$$
$$k = \frac{\nabla}{i} = \frac{1}{i}(\mathbf{e}_r \partial_r + \mathbf{e}_\phi \frac{\partial_\phi}{r}) = \mathbf{e}_r k_r + \mathbf{e}_\phi \frac{L_z}{\hbar r}.$$

$\mathbf{A}$ contains off-diagonal terms, and the diagonal term $\vec{A}_n$ is the gauge potential for $|\xi_n\rangle$. $\vec{A}_n$ results from the spatially-dependent $|\xi_n\rangle$; it is contributed only from the phase gradient of the Raman coupling's off-diagonal term $\Omega(r)e^{i\phi}$ in the spin matrix in Eq. S(1), and none from the amplitude gradient of $\Omega(r)$. The phase of $\Omega(r)e^{i\phi}$ corresponds to $\alpha = -\phi$ in Eq. S(6) and the relative phase between $\langle m_F - 1|\xi_n\rangle$ to $\langle m_F|\xi_n\rangle$. Therefore this relative phase gradient fixes the direction of $\vec{A}_n$ long $\mathbf{e}_\phi$. With this, in Eq. (2) the scalar potential is $\varepsilon_n - i\hbar\langle\xi_n|\partial_t\xi_n\rangle = \varepsilon_n$ given by a general $\beta(r,t)$ and time-independent $\alpha = -\phi$ where $i\hbar\langle\xi_n|\partial_t\xi_n\rangle = 0$.

The off-diagonal term of $\mathbf{A}$ proportional to $\hat{F}_x$ ($\hat{F}_y$) arises from the gradient of $|\xi_n\rangle$ in the phase α (amplitude depending on β). Since our dressed atoms are prepared in $|\xi_0\rangle$ and $\Delta\ell = \hbar$, we consider $n = 0, n' = -1$,

$$H_{-1,0} = -\frac{L_z\hbar}{\sqrt{2}mr^2}\sin\beta + \frac{\hbar^2}{2\sqrt{2}mr^2}\sin\beta\cos\beta - \frac{\hbar^2}{2\sqrt{2}m}\partial_r(\partial_r\beta) - \frac{\hbar^2}{2\sqrt{2}m}(\partial_r\beta)\partial_r - \frac{\hbar^2}{2\sqrt{2}mr}\partial_r\beta \tag{9}$$

and in Eq. (2),

$$H_{\text{eff}}^{(n)} = -\frac{\hbar^2}{2m}\nabla^2(r,z) + \frac{L_z^2}{2mr^2} + \frac{L_z n\hbar}{mr^2}\cos\beta + \frac{\hbar^2}{2m}\langle\nabla\xi_n|\nabla\xi_n\rangle + \varepsilon_n + V(r). \tag{10}$$

In Eq. S(10), the third term corresponds to the cross terms of L_z and rA_n in Eq. (2), and the fourth term is given by

$$\frac{(rA_n)^2}{2mr^2} + W_n = \frac{\hbar^2}{2m}\langle\nabla\xi_n|\nabla\xi_n\rangle, \tag{11}$$

, where

$$W_n = \frac{\hbar^2}{2m}(\langle\nabla\xi_n|\nabla\xi_n\rangle - i^2\langle\xi_n|\partial_\phi\xi_n\rangle^2) \tag{12a}$$
$$W_1 = W_{-1} = \frac{1}{4m}\left[\frac{\hbar^2}{r^2}\sin^2\beta + (\hbar\partial_r\beta)^2\right] \tag{12b}$$
$$W_0 = 2W_1 \tag{12c}$$

and

$$\frac{\hbar^2}{2m}\nabla\xi_1^\dagger \cdot \nabla\xi_1 = \frac{\hbar^2}{2m}\nabla\xi_{-1}^\dagger \cdot \nabla\xi_{-1} = \frac{1}{4m}\left[\frac{\hbar^2}{r^2}(1+\cos^2\beta) + (\hbar\partial_r\beta)^2\right] \tag{13a}$$
$$\frac{\hbar^2}{2m}\nabla\xi_0^\dagger \cdot \nabla\xi_0 = \frac{1}{2m}\left[\frac{\hbar^2}{r^2}\sin^2\beta + (\hbar\partial_r\beta)^2\right] \tag{13b}$$

Here we show the validity of local dressed states $|\xi_n(\vec{r},t)\rangle$ as the approximated eigenstates, and of the adiabatic condition. Consider the energies associated with the spatial gradient in both ψ and $|\xi\rangle$; they correspond to terms in Eq. S(8), leading to Eq. S(9). When these spatial gradient energies are sufficiently smaller than the energy gap $\Omega_{\text{eff}}(r)$, it gives $|H_{n'n}| \ll |\varepsilon_n - \varepsilon_{n'}| = \hbar\Omega_{\text{eff}}$ for $|n' - n| = 1$. That is, coupling between dressed states are negligible, and the adiabatic condition is fulfilled; the eigenstates of the Hamiltonian $\hat{H}_{\text{lab}}$ are well approximated by $|\xi_n(\vec{r},t)\rangle$, which are the eigenstates of $\vec{\Omega}_{\text{eff}} \cdot \vec{F}$. For our experiment of $|\xi_0\rangle$ with $\ell = 0$, the computed $|H_{-1,0}(r)|$ is smaller than $(\hbar^2/\sqrt{2}mr^2)\sin\beta\cos\beta$ for all r. We find $|H_{-1,0}(r)|$ is smaller than $\hbar\Omega_{\text{eff}}(r)$ at $r \gtrsim 0.6$ μm where the transition from $n = 0$ to $n' = -1$ is negligible.

As we include the quadratic Zeeman energy $\hbar\omega_q\hat{F}_z^2$ with $\omega_q/2\pi = 50$ Hz, it adds an offset to $(\hbar^2/2mr^2)\hat{F}_z^2$. The off-diagonal coupling $H_{-1,0}$ has an additional term $\hbar\omega_q\sin\beta\cos\beta/\sqrt{2}$, which is smaller than either $(\hbar^2/2\sqrt{2}mr^2)\sin\beta\cos\beta$ or $\hbar\Omega_{\text{eff}}(r)$, and thus the effects from $\hbar\omega_q\hat{F}_z^2$ are negligible.

Adiabaticity of the loaded dressed state

Our atoms are loaded into the eigenstate well approximated by the local dressed state $|\xi_0\rangle$ for $r > r_c$, where the adiabatic condition is fulfilled and r_c is the adiabatic radius. Using TDGPE simulations, we obtain the state after the loading, $\psi(\vec{r})|\xi(\vec{r})\rangle$. At $\delta = 0$, we compute the overlap of $|\xi(\vec{r})\rangle$ to the local dressed state $|\xi_0(\vec{r})\rangle$, where the projection probability $|\langle\xi_0(\vec{r})|\xi(\vec{r})\rangle|^2$ exceeds 0.98 at $r > r_c \approx 1.4$ μm. The energy gap $\Omega_{\text{eff}}(r)$ is sufficiently large for the small loading speed $\dot{\delta}$ and small spatial gradient energies for $r > r_c$, where the adiabatic condition holds.

Local dressed states with mean field interactions

The projected Hamiltonian $H_{\text{eff}}^{(n)}$ in Eq. (2) is for non-interacting atoms with $\omega_q = 0$. Here we include the mean field interactions $\int d^3\vec{r}n(\vec{r})\frac{1}{2}\left[c_0 n(\vec{r}) + c_2 n(\vec{r})\langle\vec{F}\rangle^2\right]$ in $F = 1$ BECs, $n = n_1 + n_0 + n_{-1}$ is the total density and n_{m_F} is the density of bare spin state $|m_F\rangle$. The coupled spinor TDGPE for $\Omega_{\text{eff}} = 0$ and $\omega_q = 0$ is

$$i\hbar\frac{\partial\Psi_1}{\partial t} = h_0\Psi_1 + c_0 n\Psi_1 + c_2(n_1 + n_0 - n_{-1})\Psi_1 + c_2\Psi_{-1}^*\Psi_0\Psi_0, \tag{14a}$$

$$i\hbar\frac{\partial\Psi_0}{\partial t} = h_0\Psi_0 + c_0 n\Psi_0 + c_2(n_1 + n_{-1})\Psi_0 + 2c_2\Psi_0^*\Psi_1\Psi_{-1}, \tag{14b}$$

$$i\hbar\frac{\partial\Psi_{-1}}{\partial t} = h_0\Psi_{-1} + c_0 n\Psi_{-1} + c_2(n_{-1} + n_0 - n_1)\Psi_{-1} + c_2\Psi_1^*\Psi_0\Psi_0, \tag{14c}$$

where $\Psi_{m_F} = \langle m_F|\Psi\rangle$, $h_0 = -(\hbar^2/2m)\nabla^2 + V(r)$, $n_{m_F} = |\Psi_{m_F}|^2$. Since the bare spin $|m_F\rangle$ is mapped to the dressed spin $|\xi_{m_F}\rangle$ by a local spin rotation $\mathcal{U}$, $|\langle\vec{F}\rangle|^2$ is invariant with respect to $\mathcal{U}$ and $|\xi_{m_F}(\vec{r},t)\rangle$ remains the eigenstates when we include the mean field.

Time evolutions

We discuss the stability of the prepared dressed atoms with the Raman fields on for a hold time $t_h > 0$. Without the interaction H_{int} and neglecting ω_q, the total Hamiltonian after the local spin rotation for removing the dependence of $\vec{\Omega}_{\text{eff}}\cdot\vec{F}$ on ϕ is

$$\hat{H}_1 = \left[\frac{-\hbar^2}{2m}\nabla^2(r,z) + \frac{L_z^2}{2mr^2} + V(r)\right]\otimes\hat{1} + \hbar\delta\hat{F}_z + \hbar\Omega\hat{F}_x + \hat{H}_{\text{SOAMC}} + \frac{\hbar^2}{2mr^2}\hat{F}_z^2.$$

When ∂_r is neglected, the eigenstates are the "modified local dressed states" $|\bar{\xi}_n(\ell,r)\rangle$ at fixed r with the good quantum number ℓ, and the wave function in the $n-$th dressed state in position representation is

$$\begin{aligned}\langle\vec{r}|\Psi\rangle &= \varphi_n(\ell,r,z)\langle\phi|\bar{\xi}_n(\ell,r)\rangle\\ &= \varphi_n(\ell,r,z)e^{i\ell\phi}U(\ell,r)|n\rangle,\end{aligned} \tag{15}$$

and $|n\rangle$ is the bare spin state. At $\ell = 0$, $|\bar{\xi}_n(\ell,r)\rangle \approx |\xi_n\rangle$ at $r \gtrsim 0.6$ μm where the effects from $(\hbar^2/2mr^2)\hat{F}_z^2$ are negligible. At large ℓ, $|\bar{\xi}_n\rangle$ deviates from $|\xi_n\rangle$ owing to the $\hat{H}_{\text{SOAMC}} = (\hbar/mr^2)\ell\hat{F}_z$.

Our dressed atoms are prepared in $|\xi_0\rangle \approx |\bar{\xi}_0\rangle$ at $\ell = 0$, where the final probability projected to $|\xi_0\rangle$ or $|\bar{\xi}_0\rangle$ is close to 1. Consider single-atom induced coupling from the initial $n = 0$ state to $n = -1$ ground dressed state. We use 2D TDGPE to simulate the state after a hold time $t_h = 0.1$ s, where it shows atoms decay to $|\bar{\xi}_{-1}\rangle$ within $|\delta|/2\pi \lesssim 0.8$ kHz. Here $\ell = 0$ remains unchanged, and we use initial states with off-centered vortex position to simulate the experiment with pointing stabilities of the laser beams. This decay is most likely due to terms with ∂_r in $\hat{H}_1$, where the initial state of the dressed atoms is close to $|\bar{\xi}_0\rangle$. If we consider the initial state as $|\xi_0\rangle$, the coupling to $|\xi_{-1}\rangle$ would be given by Eq. S(9). The actual dynamics is dictated by the prepared dressed state at $t_h = 0$ and the following evolution from the TDGPE.

Next, beyond the mean field description, we consider interactions in the second quantization form with the leading term from c_0,

$$\hat{H}_{\text{int}}^{c_0} = \frac{c_0}{2}\int d^3\vec{r}\sum_{\sigma_A,\sigma_B}\hat{\psi}_{\sigma_A}^\dagger(\vec{r})\hat{\psi}_{\sigma_B}^\dagger(\vec{r})\hat{\psi}_{\sigma_A}(\vec{r})\hat{\psi}_{\sigma_B}(\vec{r}).$$

After a Fourier transform along ϕ it becomes

$$\hat{H}_{\text{int}}^{c_0} = 2\pi\frac{c_0}{2}\int dz\int drr\sum_{\ell_1,\ell_2,\ell_3,\ell_4}\sum_{\sigma_A,\sigma_B}\delta_{\ell_1+\ell_2,\ell_3+\ell_4}\hat{\phi}_{\sigma_B}^\dagger(\ell_4)\hat{\phi}_{\sigma_A}^\dagger(\ell_3)\hat{\phi}_{\sigma_B}(\ell_2)\hat{\phi}_{\sigma_A}(\ell_1), \tag{16}$$

where $\hat{\phi}_\sigma(\ell)$ is the operator annihilating one atom with ℓ in bare spin $|m_F = \sigma\rangle$ at (r,z). $\hat{H}_{\text{int}}^{c_0}$ can couple two atoms in $|\bar{\xi}_0\rangle$ to the ground dressed state $|\bar{\xi}_{-1}\rangle$ with $\ell \neq 0$, where the energy of the initial two-atom state $|i\rangle$ matches that of the final state $|f\rangle$. Due to the nonzero ℓ acquired, $|\bar{\xi}_{-1}\rangle$ is the relevant dressed state, instead of $|\xi_{-1}\rangle$. The resonant coupling gives a decay rate of atoms prepared in $|\bar{\xi}_0\rangle$ from Fermi's golden rule (FGR). For coupling two atoms in $n=0$ to $n=-1$, we transform $H_{\rm int}^{c_0}$ to the field operators in the dressed spin basis,

$$\hat{H}_{\rm int}^{c_0} = 2\pi \frac{c_0}{2} \int dz \int drr \sum_{\ell_1,\ell_2,\ell_3,\ell_4} \delta_{\ell_1+\ell_2,\ell_3+\ell_4} \hat{\varphi}_{-1}^\dagger(\ell_4)\hat{\varphi}_0(\ell_2)\hat{\varphi}_{-1}^\dagger(\ell_3)\hat{\varphi}_0(\ell_1)$$
$$\sum_{\sigma_A,\sigma_B} U_{-1\sigma_B}^\dagger(\ell_4)U_{\sigma_B 0}(\ell_2)U_{-1\sigma_A}^\dagger(\ell_3)U_{\sigma_A 0}(\ell_1), \tag{17}$$

where $\hat{\varphi}_n(\ell)$ is the operator annihilating one atom with ℓ in dressed spin $|\bar{\xi}_n\rangle$ at (r,z),

$$\hat{\varphi}_n(\ell) = \hat{\varphi}_n(\ell,r,z), U(\ell) = U(\ell,r).$$

Given that $\ell_1 = \ell_2 = 0$ for $n=0$, $\ell_3(\ell_4) = +(-)\ell_f$ for $n=-1$ owing to $\ell_3(\ell_4) = +(-)\ell_f + \ell_{\rm min}^{(-1)} \approx +(-)\ell_f$ for $|\ell_{\rm min}^{(-1)}| < \hbar \ll \ell_f$, and $\tilde{r} \equiv (r,z)$,

$$|i\rangle = \int d\tilde{r_1} d\tilde{r_2} \varphi_0(\ell=0,\tilde{r_1})\varphi_0(\ell=0,\tilde{r_2})\frac{1}{\sqrt{2}}\hat{\varphi_0}^\dagger(\ell=0,\tilde{r_2})\hat{\varphi_0}^\dagger(\ell=0,\tilde{r_1})|0\rangle, \tag{18a}$$

$$|f\rangle = \int d\tilde{r_3} d\tilde{r_4} \frac{1}{\sqrt{2}}\left[\varphi_{-1}(\ell_f,\tilde{r_3})\varphi_{-1}(-\ell_f,\tilde{r_4}) + \varphi_{-1}(\ell_f,\tilde{r_4})\varphi_{-1}(-\ell_f,\tilde{r_3})\right]\frac{1}{\sqrt{2}}\hat{\varphi_{-1}}^\dagger(-\ell_f,\tilde{r_4})\hat{\varphi_{-1}}^\dagger(\ell_f,\tilde{r_3})|0\rangle, \tag{18b}$$

where $\varphi_0(0,\tilde{r}), \varphi_{-1}(\pm\ell_f,\tilde{r})$ are normalized single particle wave functions,

$$\int dz \int dr 2\pi r |\varphi_n(\ell,r,z)|^2 = 1.$$

This leads to the matrix element at ℓ_f

$$\langle f|H_{\rm int}^{c_0}|i\rangle_{\ell_f} = 2\pi\cdot 2\sqrt{2}\cdot\frac{c_0}{2}\int_{-z_r}^{z_r} dz \int_{\bar{r}_c}^{R_{\rm TF}} drr \varphi_{-1}^*(-\ell_f,r,z)\varphi_{-1}^*(\ell_f,r,z)\varphi_0(0,r,z)\varphi_0(0,r,z)$$
$$\left[U^\dagger(-\ell_f,r)U(0,r)\right]_{-1,0}\left[U^\dagger(\ell_f,r)U(0,r)\right]_{-1,0}. \tag{19}$$

Here $z_r = \sqrt{{R_{\rm TF}}^2 - r^2}$, $\bar{r}_c$ indicates that the atoms are prepared in $|\bar{\xi}_0\rangle$ with the probability exceeding $\bar{p}_0$ at $r > \bar{r}_c(\delta)$; $\bar{r}_c$ deviates slightly from r_c for loading into $|\xi_0\rangle$. At small detuning and $r < \bar{r}_c$ it is invalid to take the initial state as $|\bar{\xi}_0\rangle$, thus we cannot apply FGR. Here we use $\bar{p}_0 = 0.9$ to determine $\bar{r}_c(\delta)$. The motional wave functions of $|f\rangle$ are $\varphi_{-1}(\pm\ell_f)$, and

$$\left[-\frac{\hbar^2}{2m}\nabla^2(r,z) + V(r,z) + c_0 n_{\rm BEC}(r,z) + \bar{\varepsilon}(\ell_f,r) - \mu\right]\varphi_{-1}(\ell_f) = \lambda_E \varphi_{-1}(\ell_f) \tag{20}$$

with the eigenenergy λ_E which is closest to zero, since we consider the near-resonant coupling of $|i\rangle$ to $|f\rangle$. $\bar{\varepsilon}_{-1}(\ell_f,r)$ is the eigenenergy of $|\bar{\xi}_{-1}\rangle$; for $\ell_f \geq 2\hbar$,

$$\bar{\varepsilon}_{-1}(\ell_f,r) \approx \frac{\left[\ell_f - \ell_{\rm min}^{(-1)}\right]^2}{2mr^2} - \sqrt{\Omega(r)^2 + \delta^2}.$$

For $\ell_f = 0, \hbar$, $\bar{\varepsilon}_{-1}(\ell_f,r)$ is finite as $r \to 0$ while the approximated form diverges. $c_0 n_{\rm BEC}(r,z)$ is the effective potential due to interactions from most of the remaining atoms in $|\xi_0\rangle$, which is the ground state BEC with chemical potential μ. $c_0 n_{\rm BEC} = \mu - V(r,z)$ at $r < R_{\rm TF}$ and $c_0 n_{\rm BEC} = 0$ at $r < R_{\rm TF}$. We define an effective potential

$$V_{\rm eff}(r,z) = [V(r,z) - \mu]\theta(\sqrt{r^2+z^2} - R_{\rm TF}) + \frac{\left[\ell_f - \ell_{\rm min}^{(-1)}\right]^2}{2mr^2} - \sqrt{\Omega(r)^2+\delta^2}, \tag{21}$$

θ is the Heaviside step function, and

$$\left[-\frac{\hbar^2}{2m}\nabla^2(r,z) + V_{\rm eff}\right]\varphi_{-1}(\ell_f) = \lambda_E \varphi_{-1}(\ell_f). \tag{22}$$

This shows the dressed state energy $\Omega_{\rm eff} = \sqrt{\Omega(r)^2+\delta^2}$ can be converted to the sum of radial, azimuthal and axial kinetic energy. $\ell_f/\hbar \lesssim 100$ where the maximal ℓ_f corresponds to zero overlap between $\varphi_{-1}(\ell_f)$ and $\varphi_0(0)$ due to the $\ell_f^2/2mr^2$ barrier. $\varphi_0(0)$ is the ground state BEC in $|\xi_0\rangle$ with TF profile.

The spin-dependent terms in Eq. S(19) are

$$\left[U^\dagger(-\ell_f)U(0)\right]_{-1,0}\left[U^\dagger(\ell_f)U(0)\right]_{-1,0} = \langle\bar{\xi}_{-1}(-\ell_f)|\bar{\xi}_0(\ell=0)\rangle\langle\bar{\xi}_{-1}(\ell_f)|\bar{\xi}_0(\ell=0)\rangle. \tag{23}$$

This indicates the spin parts of $|\bar{\xi}_0(\ell=0)\rangle$ and $|\bar{\xi}_{-1}(\ell_f)\rangle$ are non-orthogonal, leading to the spin decay due to collisions under SOAMC. As we neglect $(\hbar^2/2mr^2)\hat{F}_z^2$ at large $r > r_c$ and take $\hat{H}_{\rm SOAMC}$ as an effective detuning $\pm\hbar\ell_f/mr^2$, $U(\ell)$ corresponds to an Euler rotation. It is $R_y(\beta)$ for $|\bar{\xi}_0\rangle$ and is $R_y(\beta_\pm)$ for $|\bar{\xi}_{-1}(\pm\ell_f)\rangle$, where $\beta_\pm$ corresponds to $\ell = \pm\ell_f$ of atoms in $|\bar{\xi}_{-1}\rangle$. Thus

$$\sum_\sigma U^\dagger_{-1\sigma}(\pm\ell_f)U_{\sigma 0}(0) = \langle -1|R_y^\dagger(\beta_\pm)R_y(\beta)|0\rangle = \frac{\sin(\beta_\pm-\beta)}{\sqrt{2}},$$

given by the off-diagonal matrix elements of $R_y^\dagger(\beta_\pm)R_y(\beta)$, and

$$\tan\beta_\pm(r,\ell_f,\delta) = \frac{\hbar\Omega/E_L}{\hbar\delta/E_L \pm 2\ell_f/\Delta\ell},$$

where $E_L(r) = \Delta\ell^2/2mr^2 = \hbar^2/2mr^2$. At large r and large $\Omega_{\rm eff}$, $|\beta_\pm - \beta|$ is small, leading to

$$\left[U^\dagger(\pm\ell_f)U(0)\right]_{-1,0} \approx \sqrt{2}\frac{\ell_f}{\hbar}\frac{E_L(r)}{\hbar\Omega_{\rm eff}}\frac{\Omega}{\Omega_{\rm eff}}. \tag{24}$$

Now we compute $\langle f|H_{\rm int}^{c_0}|i\rangle_{\ell_f}$ from Eq. S(19) and Eq. S(23). It is an overlap integral containing φ_0 for $\sqrt{r^2+z^2} < R_{\rm TF}$, within which the inner classical turning point of $\varphi_{-1}(\ell_f)$ is a z-independent $r_{\rm min}(\ell,\delta)$. The classically accessible region with $|\varphi_0|^2 > 0$ is bounded by $r_{\rm min} < r < \sqrt{R_{\rm TF}^2 - z^2}$ at given z, and $|z| < \sqrt{R_{\rm TF}^2 - r_{\rm min}^2}$. It is in the WKB regime with short wave-length $\lambda_{\rm WKB}$ and slowly varying potential, thus we only compute within the classically accessible region. In the classically forbidden region $\varphi_{-1}(\ell_f)$ exponentially decays within a short length scale $\approx \lambda_{\rm WKB}$, and thus neglected. Without numerically solving φ_{-1}, we approximate Eq. S(19) by using a dimensional analysis: we take the typical single-atom 3D density of $|\varphi_{-1}|^2$ as $\sqrt{2}/(R_z\pi(r_{\rm max}^2 - r_{\rm min}^2))$, where R_z is the typical radius along z, $r_{\rm max}, r_{\rm min}$ are the outer and inner turning points of $V_{\rm eff}(r, z=0)$, respectively; the sizes are numerically calculated as a function of (ℓ_f,δ).

The FGR is

$$\Gamma = \frac{2\pi}{\hbar}\sum_{\ell_f}\left|\langle f|H_{\rm int}^{c_0}|i\rangle_{\ell_f}\right|^2 g(E,\ell_f,\delta)N^2, \tag{25}$$

where $g(E)$ is the density of state in a trap at energy $E = \lambda_E$ (see Eq. S(20)),

$$g(E,\ell_f,\delta) = 2\pi\frac{(2m)^{3/2}}{h^3}\int d^3\vec{r}\sqrt{E - V_{\rm eff}(r,z)},$$

and N^2 factor appears since we used normalized single particle wave functions φ_0, φ_{-1}. Applying the spin-coupling terms in Eq. S(24) to Eq. S(19), and for $g(E,\ell_f)$ we make an estimate without integrating within the volume of classically accessible region: We integrate $2\pi r\sqrt{E - V_{\rm eff}(r,z)}$ within $r_{\rm min} < r < r_{\rm max}$ at $z = 0$, and then times $2\cdot R_z$ without integrating along z. We found $g(E,\ell,\delta)$ insensitive to (ℓ,δ).

DATA AND SIMULATIONS FOR THE DECAY OF DRESSED STATES

For the data of decay of dressed state $|\xi_0\rangle$ in Fig. 3, we display the fraction f_0 of the atom number in $|\bar{\xi}_0\rangle$ over the total number in $|\bar{\xi}_0\rangle$ and $|\bar{\xi}_{-1}\rangle$ at $t_h = 0.1$ s. With this normalization, the fraction would remain 1.0 with a finite one-body loss rate from spontaneous photon scattering in the Raman beams. Atoms initially in $|\bar{\xi}_0(\ell=0)$ are coupled to the energy-matched states in the ground dressed state $|\bar{\xi}_{-1}(\ell=\pm\ell_f)\rangle$ with $\ell_f > 0$, since the spin parts of $|\bar{\xi}_0(\ell=0)\rangle$ and $|\bar{\xi}_{-1}(\ell_f)\rangle$ are non-orthogonal. The fraction f_0 decays faster with decreasing $|\delta|$; near the resonance

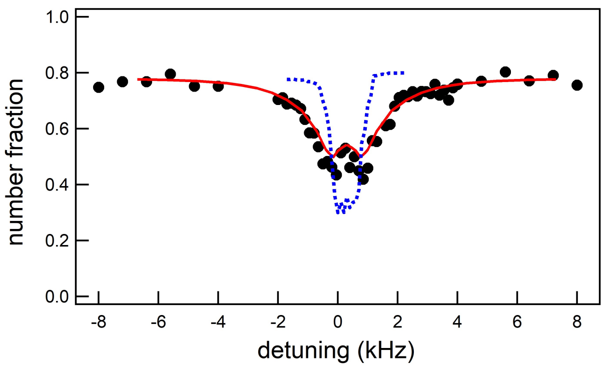

FIG. 2: Number fraction in the dressed state $|\xi_0\rangle$ after a $t_h = 0.1$ s hold time with Raman fields on versus detuning δ (symbols); the fraction is normalized to the total number at $t_h = 0.1$ s. The red curve denotes calculated loss from collision-induced decay with a correction factor. The dotted curve denotes the 2D TDGPE simulation with the vortex position off-centered by 0.5 μm in the initial state. Both simulation curves include a technical loss rate, see text.

$\delta = 0$, the lifetime reaches the minimum of 0.1 s. For $|\delta/2\pi|$ exceeding 8 kHz, $f_0(t_h = 0.1\text{ s})$ reaches $\approx 80\%$ instead of unity. This disagreement comes from experimental imperfections and can be improved with better Raman beam alignment: the loss is from the retro-reflection of one Raman beam together with the other Raman beam, which drive two-photon transitions resonant at $\delta/2\pi \sim \pm 14$ kHz, about four times the photon recoil energy.

To compare the data with simulations, we first evaluate Γ/N as described earlier, and multiply a correction scaling factor 4.2; such factor is expected given that we have used dimensional analysis for $|\varphi_{-1}|^2$ in Eq. S(19). Another possibility is that the collision may have other channels such as $|\bar{\xi}_0\rangle, |\bar{\xi}_0\rangle \rightarrow |\bar{\xi}_1\rangle, |\bar{\xi}_{-1}\rangle$ with the same order of magnitude. Γ/N is also the transition rate per atom $dN/dt/N$ at $t_h = 0$. We compare the obtained fraction $\exp[-(\Gamma/N + \gamma_0)t_h]$ at $t_h = 0.1$ s with the experimental data. Here, $\gamma_0 = 2.5\text{ s}^{-1}$ accounts for the technical loss rate corresponding to the ≈ 0.8 fraction for $t_h = 0.1$ s at large detunings (see the previous paragraph). The computed fraction is shown with the data in Fig. S2. We also compare the results with that of 2D TDGPE simulations with the vortex position off-centered by a typical value of 0.5 μm in the initial state for our experiment. This simulation shows losses within a smaller detuning range of $|\delta| \lesssim 0.8$ kHz than the data, and the curve is insensitive to the amount of off-centered vortex position between 0.2 μm to 1.0 μm. We obtain the same detuning range for a centered vortex with a small spatially random noise in the initial state. The simulation for a vortex off-centered by 0.5 μm is displayed in Fig. S2 after being multiplied by a factor of $\exp(-\gamma_0 t_h) = 0.8$. For simplicity we do not include the loss from 2D TDGPE in Fig. 3

For the simulation of Γ/N, we find at $\delta/2\pi \gtrsim 1$ kHz, the calculated rate $\Gamma(\delta)$ is insensitive to the choice of $\bar{p}_0$. While at $\delta/2\pi \lesssim 1$ kHz, the rate is notably larger with smaller $\bar{r}_c(\delta)$ set by a smaller $\bar{p}_0$. Thus, we find the approach of time-dependent perturbation and FGR are valid at $\delta/2\pi \gtrsim 1$ kHz.

NOTES ON SOAMC SYSTEMS

Cylindrical symmetry of SOAMC

In the comparison of SOAMC and SLMC with the specific case of effective rotations, or synthetic magnetic fields, leading to vortices in the ground state BEC, both schemes can achieve it. However, SOAMC can do this in a way that is cylindrically symmetric while SLMC cannot. One result of this difference is that for the lowest energy dressed state, SOAMC and SLMC give an anti-trapping potential along $\mathbf{e}_r$ and $\mathbf{e}_y$, respectively, due to the position dependent energy eigenvalues, $-\sqrt{\Omega_{\text{eff}}^2 + \delta^2}$ where $\Omega_{\text{eff}} = |\vec{\Omega}_{\text{eff}}|$.

To continue the above discussions, we compare SOAMC and SLMC with an identical synthetic magnetic field $\vec{B}^* = \nabla \times \vec{A}$, which is uniform along $\mathbf{e}_z$: In SOAMC, dressed eigenstates have angular momentum as the good quantum number, which doesnt hold for SLMC. This makes the wave functions in these two gauges have different phases, which is revealed in the measurement process when the synthetic gauge field is turned off. (see Ref. S[4]) In the usually adopted TOF method, the cloud expands symmetrically in the gauge of SOAMC, but not in that of SLMC. Here, the phase winding of the cloud is the same in both gauges although the expansion is different.

We now discuss topological spin excitations created by SOAMC. Topological spin textures with cylindrical symmetry, such as coreless vortices, skyrmions and monopoles, can not be achieved with SLMC, as we explain in the following. We consider dressed states in the spin $| < \vec{F} > | = 1$ manifold, i.e., $< \vec{F} >$ aligns with $\vec{\Omega}_{\text{eff}}$. Both spin textures of the coreless vortex and monopole have cylindrical symmetry and the direction of spin $< \vec{F} >$ winds by 2π as ϕ varies from 0 to 2π. In SLMC, the spin projected on xy plane has a helically precessing angle $2k_r x$ along $\mathbf{e}_x$, and it cannot be consistent with spin textures with cylindrical symmetry. We list examples for above statements in three cases, where we explicitly show the form of unit vector of $\vec{\Omega}_{\text{eff}}$, along which the local spin aligns. (i) $\mathbf{e}_{\text{v}}$ for a coreless vortex in SOAMC (ii) $\mathbf{e}_{\text{m}}$ for a monopole generated by spin rotations with real magnetic fields (iii) $\mathbf{e}_{\text{SLMC}}$ for the SLMC. We have

$$\begin{aligned}
\mathbf{e}_{\text{v}} &= \sin\beta(r)\cos\phi\mathbf{e}_x - \sin\beta(r)\sin\phi\mathbf{e}_y + \cos\beta(r)\mathbf{e}_z, \\
\mathbf{e}_{\text{m}} &= \sin\theta^{'}\cos\phi^{'}\mathbf{e}_x + \sin\theta^{'}\sin\phi^{'}\mathbf{e}_y - \cos\theta^{'}\mathbf{e}_z, \\
\mathbf{e}_{\text{SLMC}} &= \sin\beta_1(y)\cos[2k_r x]\mathbf{e}_x - \sin\beta_1(y)\sin[2k_r x]\mathbf{e}_y + \cos\beta_1(y)\mathbf{e}_z.
\end{aligned}$$

For (i), $\beta(r) = \tan^{-1}[\Omega(r)/\delta]$ and δ is spatially uniform; for (ii), $(r^{'}, \theta^{'}, \phi^{'})$ is a rescaled spherical coordinate from $(x^{'} = x, y^{'} = y, z^{'} = 2z)$ (see Ref. S[5]). For (iii), $\beta_1(y) = \tan^{-1}[\Omega/\delta_1(y)]$ where Ω is spatially uniform and $\hbar k_r$ is the photon recoil momentum.

Next we discuss the comparison of SOAMC to spin rotations with real magnetic fields $\vec{B}$ for making topological excitations, and potential studies on those with SOAMC. Since $\vec{\Omega}_{\text{eff}}$ with SOAMC can be designed with a spatial-light-modulator or digital-mirror-device, it can have smaller spatial scales and faster time scales as compared to those of spin rotations with real magnetic fields, whose spatial scale is determined by the coil size and time scale is limited by the coil's inductance. One obvious advantage from small spatial scales is the capability of studying interactions within a pair of vortex-antivortex, or a pair of monopole-antimonopole, where probing a small pair size may be possible. Here, we refer to monopoles (antimonopoles) as those generated by real (light-induced) magnetic fields with $\nabla \cdot \vec{B} = 0$ $(\nabla \cdot \vec{\Omega}_{\text{eff}} \neq 0)$. The topological charge is given by the surface integral

$$Q = \frac{1}{4\pi} \int d\theta d\phi \; \hat{b} \cdot \left(\partial_\theta \hat{b} \times \partial_\phi \hat{b} \right),$$

where $\hat{b}$ is the unit vector of local $\vec{B}$ or $\vec{\Omega}_{\text{eff}}$. Consider a monopole with $\hat{b} = \hat{b}_{\text{m}}$ and an antimonopole with $\hat{b} = \hat{b}_{\text{am}}$, where

$$\hat{b}_{\text{m}} = \frac{x^{'}\mathbf{e}_{x'} + y^{'}\mathbf{e}_{y'} - z^{'}\mathbf{e}_{z'}}{r^{'}}, \hat{b}_{\text{am}} = \frac{x^{'}\mathbf{e}_{x'} + y^{'}\mathbf{e}_{y'} + z^{'}\mathbf{e}_{z'}}{r^{'}}.$$

The nonzero divergence of $\hat{b}_{\text{am}}$ is made possible by $\vec{\Omega}_{\text{eff}}$ with SOAMC. One can easily check that the topological charge Q for the monopole (antimonopole) is negative (positive). If we make a sign change, $\hat{b}_{\text{m}} \to -\hat{b}_{\text{m}}$, and $\hat{b}_{\text{am}} \to -\hat{b}_{\text{am}}$, the sign of the topological charge changes for both the monopole and antimonopole, while the antimonopoles always have opposite charges to that of the monopoles which are generated by real magnetic fields.

We now discuss examples of topological excitations that can be generated by $\vec{\Omega}_{\text{eff}}$ with SOAMC, which are not achievable in a straightforward way by spin rotations with real magnetic fields. As mentioned previously, two examples are a pair of monopole-antimonopole, and a pair of vortices or vortex-antivortex. The latter can be created with two pairs of LG Raman beams; when the propagating directions of these two pairs are not colinear, one can study the collisions of non-colinear vortices. For instance, the production of resulting rung vortex for non-abelian vortices in the $F = 2$ manifold can be tested.

Proposal of measuring superfluid fractions with SOAMC

We discuss the scheme of measuring superfluid (SF) fractions with SOAMC in Ref. S[6] using a spectroscopy method, i.e., the population imbalance of bare spin components after projection of the dressed state. As we will show, such measurement cannot be used to derive SF fractions with the SLMC, owing to the spin imbalance is gauge-dependent.

In Ref. S[6], $F = 1$ atoms are confined in a ring trap with radius R under SOAMC in the lowest energy dressed state, which is consistent with $|\bar{\xi}_{-1}\rangle$ in our notation. With a Raman detuning δ, the effective energy dispersion of the dressed state is $(\ell - \ell^*)^2/2m^* R^2$, where the minimum is at $\ell = \ell^*(\delta)$, corresponding to an effective rotation and an azimuthal gauge potential. Here it is in the large Raman coupling regime, $\hbar\Omega/E_L \gg 1$, $E_L = \Delta\ell^2/2mR^2$, and the effective mass is $m^* = m(1 + 2E_L/\hbar\Omega)$. The minimum is

$$\ell^* \approx \frac{\delta}{\Omega}\Delta\ell \tag{26}$$

for small δ/Ω. One can derive the population imbalance between the bare spin components $|m_F = -1\rangle$ and $|m_F = 1\rangle$ as

$$|\psi_{-1}|^2 - |\psi_1|^2 = \frac{\ell}{\Delta\ell} - \frac{\ell - \ell^*}{(m^*/m)\Delta\ell} = \Delta p_0 + \Delta p^{'}\ell, \tag{27a}$$

$$\Delta p_0 \approx \frac{\delta}{\Omega}\left(1 - \frac{2E_L}{\hbar\Omega}\right), \tag{27b}$$

$$\Delta p^{'} \approx \frac{1}{\Delta\ell}\frac{2E_L}{\hbar\Omega}. \tag{27c}$$

The SF has $\ell = 0$ and the population imbalance $\Delta p = \Delta p_0$; the normal fluid has $\ell = \ell^*$ with zero velocity and $\Delta p_N \neq \Delta p_0$. To experimentally measure the SF fraction, one needs to distinguish a SF from a normal fluid, i.e., to measure the Δp with an absolute accuracy of $\Delta p_N - \Delta p_0$.

Now we consider the SF and normal fluid under SLMC, where the Raman coupling Ω_1 is uniform and the detuning $\delta_1(y) = \delta_1^{'} y$ has a gradient. Similar to Eq. S(27), the population imbalance of the bare spin components of the dressed state is

$$|\psi_{-1}|^2 - |\psi_1|^2 = \frac{k_x}{2k_r} - \frac{k_x - k_x^*}{(m_1^*/m)2k_r}, \tag{28}$$

where $\hbar k_x$ is the x component of canonical momentum $\vec{P}_{\text{can}}$ and $k_x^* = -B^* y/\hbar$ is the minimum location of the energy dispersion versus k_x; B^* is the strength of the approximately uniform synthetic magnetic field along z, and $m_1^* = m(1 + 2E_L/\hbar\Omega_1)$. For the SF, one can derive [4]

$$\vec{P}_{\text{can}} = -\frac{B^* y}{2}\mathbf{e}_x - \frac{B^* x}{2}\mathbf{e}_y. \tag{29}$$

The SF has the spin population imbalance

$$\Delta s_0 = \frac{B^* y}{4\hbar k_r}\frac{2E_L}{\hbar\Omega_1}. \tag{30}$$

A normal fluid has the ensemble averaged $\langle k_x\rangle - k_x^* = 0$, and thus $\langle k_x\rangle = k_x^*$, leading to

$$\Delta s_N = \frac{B^* y}{2\hbar k_r}. \tag{31}$$

Thus, for both the SF and normal fluid, with the spectroscopy method the spin population imbalance is zero after being summed within the atomic cloud.

Practical schemes for realizing the striped phase

The characteristic energy scale in SOAMC systems is $E_L = \Delta\ell^2/2mR^2$, where $\Delta\ell$ is the OAM transfer from the Raman beams and R is the typical system size. For $\Delta\ell = \hbar$ and $R = 5\ \mu$m, $E_L = h \times 2.3$ Hz is much smaller than that of SLMC, $E_r \approx h \times 3.5$ kHz at $\lambda = 0.8\ \mu$m.

For observing the stripe phase in SOAMC, an example with typical experimental parameters is shown in Ref. S[7]. Here, pseudo-spin 1/2 ^{87}Rb BECs with Thomas-Fermi radius about 40 μm have SOAMC with two Raman LG beams carrying phase winding numbers of ± 2, and the OAM transfer is $\Delta\ell = 4\hbar$. The radius at peak intensity of both LG beams is $r_M =$ 17 μm. At zero Raman detuning, the critical peak Raman coupling is $h \times 0.8$ Hz for the transition between the striped phase (miscible) and the immiscible phase; here $E_L = h \times 0.6$ Hz.

The critical Raman coupling $\hbar\Omega_c$ at the order of $h \times 1$ Hz is not practical for experiments given that the detuning noise arising from typical magnetic field noise of 1 mG is $h \times 700$ Hz. Therefore, one needs to increase E_L and thus Ω_c. From Ref. S[8], single high-order LG beam with phase winding number of 100 can be made with a SLM. An estimate

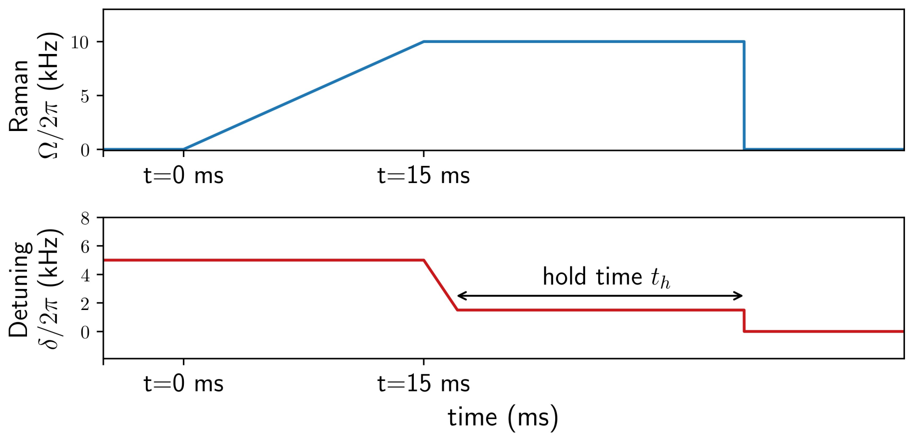

FIG. 3: Time sequences of the Raman coupling and detuning for loading atoms into the dressed state.

of $\hbar\Omega_c$ for observing miscible stripe phases can be $\gtrsim h \times 1$ kHz for $\Delta\ell = 50\hbar$ and a condensate radius of 10 μm. Here we scale down the size of the condensate and the radius at peak intensity of the Raman LG beams from those in Ref. S[7]; the LG beams carry phase winding number of ± 25, respectively. Consider the effects of detuning noise arising from magnetic field noise, one can expect to suppress the noise to $\sim h \times 100$ Hz, or 0.14 mG. For reaching field noise below $h \times 100$ Hz, see Ref. S[9]. The corresponding detuning noise can be made much smaller than the critical Raman coupling. Combining all these numbers it suggests that observing miscible stripe phases in SOAMC system may be possible. (Note that the parameters of phase winding number of 25 and the scaled-down $r_M = 4.25$ μm corresponds to a waist of $w = r_M/\sqrt{25/2} = 1.2$ μm, which is close to the diffraction limit given $\lambda = 0.8$ μm. Thus one needs to use a high numerical-aperture imaging objective.)

METHODS OF THE EXPERIMENT

System preparation and probing

We produce a ^{87}Rb BEC of $N \approx 4 \times 10^5$ atoms in a crossed dipole trap in $|1, -1\rangle$ with approaches similar to those in Ref. [10]. The dipole trap contains two 1064 nm laser beams propagating along $\mathbf{e}_{x'}, \mathbf{e}_{y'} = (\mathbf{e}_x \pm \mathbf{e}_y)/\sqrt{2}$ with beam waists of ~ 65 μm, and the trap frequencies for the BEC are $(\omega_{x'}, \omega_{y'}, \omega_z)/2\pi$=(72,72,81) Hz. After the BEC production we wait for the external trigger from the 60 Hz line, after which we apply feed-forward current signals into bias coils to cancel the field noise from 60 Hz harmonics (see later discussions). Then we transfer the BEC to $|1, 0\rangle$ by first applying a microwave π pulse at $|1, -1\rangle \rightarrow |2, 0\rangle$ transition, followed by a second π pulse at $|2, 0\rangle \rightarrow |1, 0\rangle$. We confirm there were no discernible atoms left in $|1, -1\rangle$, and blow away the residual $|2, 0\rangle$ atoms with a resonant $F = 2 \rightarrow F^{'} = 3$ pulse. We then again wait for the 60 Hz trigger, and load the atoms into the Raman dressed state with the following procedures. We ramp the detuning to $\delta/2\pi = 5$ kHz while the Raman beams are off, ramp $\Omega(r, t)$ in 15 ms to the final value of $\Omega_M/2\pi = 10$ kHz, and then ramp the detuning to $\delta_f/2\pi$ between 4 kHz and -1 kHz with $\dot{\delta}/2\pi = -1.67$ kHz/ms (see Fig. S3), subsequently holding Ω_M and δ at constant for t_h. The Raman beams are at $\lambda = 790$ nm where their scalar light shifts from the D1 and D2 lines cancel. The Gaussian Raman beam has a waist of 200 μm, and the LG Raman beam produced by a vortex phase plate has a phase winding number $m_\ell = 1$ and radial index of 0. The Raman beams are linearly polarized along $\mathbf{e}_x$ and $\mathbf{e}_y$, respectively.

For projection measurements of the spinor state $|\xi_s\rangle$, we abruptly turn off the dipole trap and Raman beams, simultaneously and adiabatically rotate the magnetic bias field from along $\mathbf{e}_x$ to that along the imaging beam direction within 0.4 ms; this projects $|\xi_s\rangle$ to the bare spin m_F basis. The atoms then expand in free space with all m_F components together for a time-of-flight (TOF). To perform spin-selective imaging, we apply a microwave pulse to drive the $|1, -1\rangle \rightarrow |2, -2\rangle$ transition for imaging $m_F = -1$, $|1, 0\rangle \rightarrow |2, 0\rangle$ pulse for imaging $m_F = 0$, and $|1, 1\rangle \rightarrow |2, 2\rangle$ for imaging $m_F = +1$, respectively. These three frequencies are separated by 0.91 MHz in a field ~ 1.3 G along $\mathbf{e}_z$ for the vertical imaging and by 0.42 MHz in ~ 0.6 G along $\mathbf{e}_y$ for the side imaging. The resonances have separations much larger than the microwave Rabi frequencies, which are between 4.3 and 16 kHz. After the $F = 1$ atoms are transferred to $F = 2$, we apply a resonant absorption imaging pulse of ~ 14 μs with $\sigma+$ polarization at the $|F = 2, m_F = 2\rangle \rightarrow |F^{'} = 3, m_F = 3\rangle$ cycling transition. The saturation parameter is $I/I_s = 1.60$ for the vertical imaging and $I/I_s = 0.66$ for the side imaging. We use the modified Beer-Lamberet law [11] to derive correct optical densities.

The ambient field noise has a standard deviation $(\sigma) \sim h \times 0.6$ kHz, which is dominated by the 60 Hz line signal and its high-order harmonics. After we apply feed-forward signals in the bias fields to cancel the dominating field noise at 60 Hz, 180 Hz, and 300 Hz, the $1-\sigma$ residual field noise is ~ 0.2 kHz. We prepare the dressed state after the 60 Hz line trigger in order to reduce the shot-to-shot field variation with a fixed hold time after the trigger. The measured $1-\sigma$ field noise from repeated experimental shots is ~ 0.11 kHz.

Interference for measuring relative phases

We prepare the $\vec{F} = 0$ polar dressed state at $\delta = 0$, hold $t_h = 1$ ms, and then apply a radio-frequency(rf) $\pi/2$ pulse which transforms the $|1, \ell_1\rangle$ component to $(|1, \ell_1\rangle/2 + |0, \ell_1\rangle/\sqrt{2} + |-1, \ell_1\rangle/2)^T$, and the $|-1, \ell_{-1}\rangle$ component to $(|1, \ell_{-1}\rangle/2 - |0, \ell_{-1}\rangle/\sqrt{2} + |-1, \ell_{-1}\rangle/2)^T$. This mixed angular momentum states ℓ_1 and ℓ_{-1} into each spin state for interference. After TOF we selectively probe the $|1\rangle$ component; the nodal-line in Fig. 1c shows $|\ell_1 - \ell_{-1}| = 2\hbar$ and the relative phase winding between $|1\rangle$ and $|-1\rangle$ components of the dressed state is 4π. This is under the condition when the two Raman beams are aligned to be co-propagating; when their propagating directions deviated slightly the interference showed a fork-pattern like those in [12].

Deloading

To measure the dressed atoms' projections onto individual dressed bands by deloading, we reverse the loading sequence: we ramp the detuning back to the initial value of $\delta/2\pi = 5$ kHz with $\dot{\delta}/2\pi = 1.67$ kHz/ms, turn off Ω in 15 ms, and start TOF. Thus, for $r > r_c$ where it is adiabatic given the ramping speed and a sufficiently large energy gap $\Omega_{\text{eff}}(r)$, atoms in the dressed bands $|\bar{\xi}_1(r)\rangle, |\bar{\xi}_0(r)\rangle, |\bar{\xi}_{-1}(r)\rangle$ are mapped to the bare spin states $|+1\rangle, |0\rangle, |-1\rangle$, respectively [13, 14]. We apply Stern-Gerlach gradient during TOF, and use a repumping laser to pump the atoms from $|F = 1\rangle$ to $|F = 2\rangle$ before the absorption imaging.

Consider the condensate component before TOF starts. For dressed atoms with the external part of wave function $\varphi_{n,\ell}(r, z)$ and the normalized spinor state $|\bar{\xi}_n(\ell, r)\rangle$ in Eq. S(15), it is mapped to the bare spin $|m_F = n, \ell + n\hbar\rangle$ with the external wave function unchanged. This mapping is valid when the δ-dependent light shift potentials ε_n of the dressed state for $n = \pm 1$ are not so large to deform the external wave function during the ramping of δ in deloading. After TOF starts, if all the spin components expand together, after the expansion each spin corresponds to a dilation of the in-situ profile by the same factor under the approximation of neglected c_2, which is verified by the TOF simulations (Fig. S1). In the case with Stern-Gerlach gradient which spatially separates the spin components, the dilation does not apply while the respective number in each dressed state are mapped to respective bare spin states. Finally we consider the thermal component resulting from the collisional relaxation from $|\bar{\xi}_0\rangle$ to $|\bar{\xi}_{-1}\rangle$: after TOF it gives momentum distributions of each spin component regardless whether the Stern-Gerlach gradient is applied, provided the interaction during TOF is neglected.

DATA ACQUISITION AND ANALYSIS

For data in Fig. 2 and Fig. 4, the imaging is performed with the microwave spectroscopy selective to the bare spin m_F. i.e., each m_F image corresponds to an individual experimental realization. The deloading data in Fig. 3 is taken with Stern-Gerlach gradient during TOF, where images of all spin $|m_F\rangle$ states are taken in a single shot (see inset).

For Fig. 2 data, we average over about 10 images taken under identical conditions; this takes into account the shot-to-shot BEC number variation with a standard deviation $(\sigma) \sim 3$ %, and reduces the photon shot noise. In Fig. 2a, the shaded region indicates the standard deviation between the about 10 images, where it doesn't take into account the variations along $\mathbf{e}_\phi$. Given the short-term pointing stability of the dipole beams and of the Raman LG beam which determine the center of BEC and vortices, respectively, we post-select images whose vortex positions in $|m_F = \pm 1\rangle$ with respect to the BEC center are < 0.63 μm (converted from TOF position to in-situ position). We determine $\delta/2\pi$ from the rf-spectroscopy with an uncertainty of $\lesssim 0.1$ kHz. With the given field noise at a fixed

$t_h = 1$ ms, we post-select images whose optical density of the $|0\rangle$ component are within one σ; this excludes data with large variation of δ.

In Fig. 2a, at $\delta = 0$ the measured spin texture fraction of $|m_F = 0\rangle$ $D_0/(D_1+D_0+D_{-1})$ is about 0.1 at $r = 0$, which is much smaller than the expected 1.0, since the vortices in $|\pm 1\rangle$ ideally have the optical densities $D_{-1} = D_1 = 0$ at $r = 0$. This is consistent with the observation that D_0's $1/e^2$ radius is larger than the ≈ 90 μm BEC radius (after TOF), and much larger than the ≈ 15 μm predicted by TOF simulations (see Fig. S1a). This disagreement is likely due to that at exact resonance, $\delta = 0$, the dressed state loading is affected by technical noises in the Raman beams and the small non-adiabatic spin fraction deviates from the prediction.

For data in Fig. 4, from individually taken images of $|m_F = \pm 1\rangle$, we post select those whose BEC centers are sufficiently close before the Raman beam is turned off, in the presence of the dipole beam's point stability. We collect 10 images from individual experimental realizations for both $|1\rangle$ and $|-1\rangle$ (D_0 is not discernible), take the sum of total optical density $D_1 + D_{-1}$ from the $10^2 = 100$ combinations, and fit them to 2D TF profiles. We select the pair with best fit for each $t_{\rm on}$ and display them in Fig. 4. For a given $t_{\rm on}$, we find that about three best- fit pairs have similar magnetization images and are thus representative, indicating such post-selection is effective.

* Electronic address: linyj@gate.sinica.edu.tw

[1] T.-L. Ho, Physical Review Letters **81**, 742 (1998).
[2] Y. Kawaguchi and M. Ueda, Physics Reports **520**, 253 (2012).
[3] I. B. Spielman, in *Annual Review of Cold Atoms and Molecules* (WORLD SCIENTIFIC, 2013), pp. 145–187.
[4] L. J. LeBlanc, K. Jiménez-García, R. A. Williams, M. C. Beeler, W. D. Phillips, and I. B. Spielman, New Journal of Physics **17**, 065016 (2015).
[5] M. W. Ray, E. Ruokokoski, S. Kandel, M. Möttönen, and D. S. Hall, Nature **505**, 657 (2014).
[6] N. R. Cooper and Z. Hadzibabic, Physical Review Letters **104**, 030401 (2010).
[7] C. Qu, K. Sun, and C. Zhang, Physical Review A **91**, 053630 (2015).
[8] S. Moulder, Ph.D. thesis, University of Cambridge (2013).
[9] D. Trypogeorgos, A. Valdés-Curiel, N. Lundblad, and I. B. Spielman, Physical Review A **97**, 013407 (2018).
[10] Y.-J. Lin, A. R. Perry, R. L. Compton, I. B. Spielman, and J. V. Porto, Phys. Rev. A **79**, 063631 (2009).
[11] G. Reinaudi, T. Lahaye, Z. Wang, and D. Guéry-Odelin, Optics Letters **32**, 3143 (2007).
[12] J.-Y. Choi, W. J. Kwon, and Y.-I. Shin, Physical Review Letters **108**, 035301 (2012).
[13] R. A. Williams, L. J. LeBlanc, K. Jiménez-García, M. C. Beeler, A. R. Perry, W. D. Phillips, , and I. B. Spielman, Science **335**, 314 (2012).
[14] Y.-J. Lin, R. L. Compton, K. Jiménez-García, W. D. Phillips, J. V. Porto, and I. B. Spielman, Nature Physics **7**, 531 (2011).